UCONN LIBRARY

University of Connecticut
OpenCommons@UConn

Honors Scholar Theses | Honors Scholar Program

Spring 5-8-2011

Development of a Phase Separation Model for a Biodiesel Reactor

Lu Han
University of Connecticut - Storrs, lu.han1716@gmail.com

Follow this and additional works at: https://opencommons.uconn.edu/srhonors_theses

 Part of the Chemical Engineering Commons

Recommended Citation
Han, Lu, "Development of a Phase Separation Model for a Biodiesel Reactor" (2011). *Honors Scholar Theses*. 170.
https://opencommons.uconn.edu/srhonors_theses/170

Development of a Phase Separation Model for a Biodiesel Reactor

Lu Han

An Honors Thesis

Department of Chemical, Materials, and Biomolecular Engineering

Research Advisors: Richard Parnas and James Stuart

Contents

Abstract

The goal of this work is to establish a phase separation model for a biodiesel system, for the purpose of modeling a continuous flow multiphase biodiesel reactor. The Cahn-Hilliard theory is applied for a ternary system of two immiscible components and a third partially miscible component. The results of this work shows that phase field theory can be applied in phase modeling of a biodiesel system, and further investigations are required to develop a comprehensive biodiesel reactor model.

I. Introduction

A. Biodiesel Background

The derivation of energy from alternative sources becomes ever more important in scientific research given the exhausting use of fossil fuels and damage to the global ecosystem. The production of hydrocarbon fuels from biomass has many important sustainable advantages and requirements. First, "green" hydrocarbon fuels need to be essentially the same as those currently derived from petroleum-based fuels, except that they are made from biomass [1]. Therefore, existing infrastructure will not need to be modified and hydrocarbon bio-refining processes can be combined with fuel production systems of existing petroleum refineries. Second, biomass-based hydrocarbon fuels have equivalent energy units to fuels derived from petroleum, so there will be no gas-mileage penalty. Third, the source of the biomass-based fuels should not compete with food products, and fourth that the production of "green fuel" should require less energy to make and that the final price to the consumer will be as or more attractive than petro-products.

Biodiesel has been shown to meet the above sustainability requirements in climate change mitigation, human rights, food security, and natural resource conservation, according to the National Biodiesel Board (NBB). Biodiesel is one of the most diverse fuels available, because it is derived regionally from available, renewable resources, including vegetable oil, recycled restaurant grease, and animal fats. A study by the National Renewable Energy Laboratory found that the domestic feedstocks for biodiesel totaled 1.6 billion gallons and anticipates the natural growth and expansion of existing feedstocks (soy, canola, and sunflower) could expand for an additional 1.8 billion gallons by 2016. The increased demand for biodiesel is stimulating research and investment in developing new materials to make biodiesel, such as algae, camelina, jatropha, other arid land crops, and waste materials like trap grease. Ideally the increase in feedstock volumes would come from using low-production lands and utilizing innovative technologies.

The Energy Independence and Security Act of 2007 (EISA 2007) mandates the production of 36 billion gallons per year production of biofuels by 2022, of which 21 million must come from feedstock other than corn starch [2]. There have been warnings of rising food prices due to the increased competition with the food industry. However, U.S. biodiesel has a very a small impact on food costs. In the past year, food prices have risen 5.1%; only an estimated 0.2-0.6% of that total increase has been contributed to biofuels (biodiesel, ethanol, cellulosic ethanol) production, according to the U.S. Department of Agriculture (USDA). The leading factor to global grain price inflation is the rising cost of crude oil, which over a four-year period, has more than tripled from $40/barrel to nearly $150/barrel in July of 2008 [3]. This has led to increased costs to farmers for fertilizer, harvest, and transportation. Other contributing factors are the increased demand as the populations of developing countries continue to rapidly multiply and that these populations improve their diets. Also, there have been two years of bad weather and severe regional droughts leading to poor harvests in parts of the world, and export restrictions imposed by some countries. Thus, it is the high price of energy and other reasons that drive the higher food prices, not greater demand for soy and other food grains.

It has been reported that biodiesel has the highest energy balance of any transportation fuel. The University of Idaho and US Department of Agriculture showed that for every unit of fossil fuel needed to produce biodiesel, 4.5 units of energy are returned. This calculation took into account the expenditure of the energy needed for efficient planting, harvesting, fuel production, and fuel transportation of modern technologies. In the production of biodiesel, crops are not irrigated or planted solely to produce biodiesel. In 1998, the US Departments of Agriculture and Energy found from a life cycle assessment that biodiesel's production reduced wastewater by 79% and reduced hazardous waste production by 96% compared to petroleum diesel. The adoption of biodiesel production can recycle commercial and agricultural wastes, bring sustainable agriculture to marginal lands, increase crop yields, and further lower pesticide and fertilizer applications.

Currently, biodiesel is registered as a fuel and fuel additive with the Environmental Protection Agency (EPA) and meets clean diesel standards established by the California Air Resources Board (CARB). Pure biodiesel has been designated as an alternative fuel by the Department of Energy (DOE) and the U.S. Department of Transportation (DOT). Moreover, in December 2001, the American Society of Testing and Materials (ASTM) approved a specification (D6751) for biodiesel fuel. This development was crucial in standardizing fuel quality for biodiesel in the U.S. market. As of 2008, ASTM also instituted D975 as the specification for B5 and B6-B20 for blends of biodiesel mixed with petroleum diesel. The biodiesel industry also utilizes a voluntary quality management certification program for biodiesel producers, marketers, and laboratories called the BQ-9000 Program. The BQ-9000 Program combines internationally accepted quality management principles with the ASTM biodiesel fuel specification to help ensure that customers and end users get the highest quality fuel possible. The National Biodiesel Accreditation Commissions issues 'BQ-9000 Marketer,''BQ-9000 Producer' and 'BQ-9000 lab' certifications for biodiesel marketers and/or producers and biodiesel testing laboratories that have met all requirements of quality management system certification program. BQ-9000 companies are subject to annual third-party audits to verify their continued compliance with the program requirements. The BQ-9000 program provides added assurance to customers, as well as engine manufacturers, that the biodiesel marketed by these companies meets the ASTM standards for biodiesel and that the fuel supplier will stand behind its products [4].

Biodiesel has similar operational performance as that of low-sulfur diesel, and blends with petroleum diesel do not require modification of existing engines or dispensing infrastructures. Biodiesel has a higher cetane number than most U.S. diesel fuel. In more than 500 million on-road miles and countless marine and off-road applications, biodiesel shows similar fuel consumption, horsepower, torque, and haulage rates as conventional diesel fuel. Blending of biodiesel and diesel improves engine

lubricity. Even biodiesel levels as low as one percent can provide up to a 65% increase in lubricity in distillate fuels [5].

Aside from the operational compatibility with petro-diesel, biodiesel offers health benefits. Biodiesel emissions have decreased levels of all target polycyclic aromatic hydrocarbons (PAH) and nitrited PAH compounds, as compared to petroleum diesel exhaust. PAH and nPAH compounds have been identified as potential cancer causing compounds. Targeted PAH compounds were reduced by 75 to 85%, with the exception of benzo(a)anthracene, which was reduced by roughly 50%. Target nPAH compounds were also reduced dramatically with biodiesel fuel, with 2-nitrofluorene and 1-nitropyrene reduced by 90 percent, and the rest of the nPAH compounds reduced to only trace levels. All of these reductions are due to the fact the Biodiesel fuel contains no aromatic compounds.The use of biodiesel also has proven to reduce dangerous emissions, which contribute to climate change. From a life cycle analysis, there is no net overall generation of carbon to the environment, and carbon dioxide emissions are reduced by 78% compared to petroleum diesel. The carbon dioxide released into the atmosphere when biodiesel is burned is recycled by growing plants, which are later processed into fuel [6]. That study found that B20 (20% biodiesel blended with 80% conventional diesel fuel) reduced total hydrocarbons by up to 30%, carbon monoxide up to 20%, and total particulate matter up to 15%. Research also documents the fact that the ozone forming potential of the hydrocarbon emissions of pure biodiesel is nearly 50% less than that of petroleum fuel. Pure biodiesel does not contain sulfur and therefore reduces sulfur dioxide exhaust from diesel engines to virtually zero [3].

As it is grown and processed domestically, biodiesel can reduce America's dependence on foreign oil and expand domestic economy. The 500 million gallons of biodiesel produced in the U.S. in 2007 displaced 20 million barrels of petroleum, and with the increased production and use of biodiesel, the further dependence on petroleum oil is expected to be displaced [3]. The biodiesel industry has

contributed significantly to the domestic economy. The 51,893 jobs that are currently supported by the US biodiesel industry reflect the beginning of the industry's potential to create jobs and economic growth in the American economy. Biodiesel has added $4.287 billion to the Gross Domestic Product (GDP). Biodiesel has the potential to support more than 78,000 jobs by 2012. A stable, thriving biodiesel industry is necessary if the U.S. is to eventually benefit from the commercial scale production of algal-based biofuels. The National Biodiesel Board (NBB) estimates that for every 100 million gallons of biodiesel that is produced from algae, 16,455 jobs will be created and $1.461 billion will be added to the GDP [4].

B. Reaction

Biodiesel is manufactured through a transesterification reaction of triglycerides, which are the oils found in biomass and sometimes animals, using methanol or other higher alcohols. The transesterification reaction is typically catalyzed using a base, most commonly sodium hydroxide or potassium hydroxide. When mixed with methanol the potassium hydroxide molecule (or sodium hydroxide) dissociates and allow for the presence of methoxide in equilibrium concentrations as governed by the dissociation reaction. This methoxide molecule can then cleave the triglyceride (via nucleophillic attack of the carbonyl group) to form a fatty acid methyl ester (FAME) which is commonly known as Biodiesel [7]. The overall reaction is shown below, where the -R represents a hydrocarbon chain.

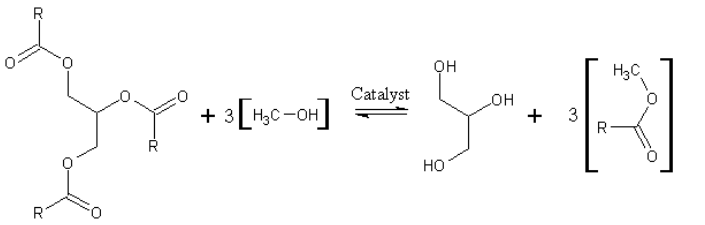

Actually, the production of biodiesel occurs in three stepwise equilibrium reactions. The first reaction is the conversion of triglyceride (TG) to digylceride (DG). The second reaction is the conversion of DG to monoglyceride (MG). The final reaction is the conversion of MG to glycerol (GL). In each reaction, a single molecule of FAME is formed.

$CH_3OH + TG \leftrightarrow DG + FAME$

$CH_3OH + DG \leftrightarrow MG + FAME$

$Ch_3OH + MG \leftrightarrow GL + FAME$

C. Novel Continuous Flow Biodiesel Reactor

The majority of current biodiesel production methods employ batch reactor technology, which limits the capacity and extends reacting time, thereby significantly adding to the total cost. Owing to the immiscibility of triglycerides and methanol, and also biodiesel and glycerol, the synthesis of biodiesel takes place as a two-phase reaction. Batch reactors utilize intense mixing to create and maintain a stable emulsion in order to minimize mass transfer limitations and to allow the reaction to reach kinetic equilibrium. Under batch operation, subsequent separation stages are required to remove the co-product glycerol and methanol from the biodiesel product. Additionally, due to stringent ASTM specifications for free and total glycerin content, the equilibrium conversion obtained in a batch system often does not meet ASTM fuel standards, due to an excess of partially reacted glycerides.

The inefficiencies of a batch reactor can be reduced by implementing continuous removal of the glycerol phase during the reaction, which will drive the equilibrium reaction to completion. The existing technologies capable of glycerol phase separation necessitate a large input of energy for separation and purification processes, thereby introducing substantial energy costs. The novel continuous reactor/separator, patented by University of Connecticut's Professor Richard Parnas, his associates, and their students, employs a static mixing unit as an injector to a reaction chamber, which relieves the need for extreme conditioned mixing [8]. The vegetable oil is preheated to about 50°C and combined with a

mixture of methanol and potassium hydroxide, the feed is fed from the bottom plate of the reactor and allowed to flow through tortuous pathways in the static mixer. The flow rate in the reactor is kept low enough to ensure a laminar flow regime in order to allow glycerol to partition out of solution. As the reactants flow upward through the tubular reactor, the formed glycerol molecules separate by density from the organic phase and settle downward, where they coalesce into a homogenous glycerol phase at the bottom. The continuous removal of glycerol at the bottom and biodiesel from the top of the reactor drives the equilibrium towards completion. **Figure 1** is a schematic of the reactor. The reactor column stands 48 inches high and has an inner diameter of 6 inches. Representative feed flow rates into the reactor for normal steady state operation are approximately 15 gal/hr (57 L/hr) of vegetable oil and 0.055 gal/min (0.21 L/min) of methanol. These conditions result in a bulk feed velocity of about 0.055 in/s (0.0014 m/s) and a space time of ~866 sec [7]. The reactor has achieved greater than 99% conversion of pre-treated waste canola oil to biodiesel by removing 70-99% of glycerol produced.

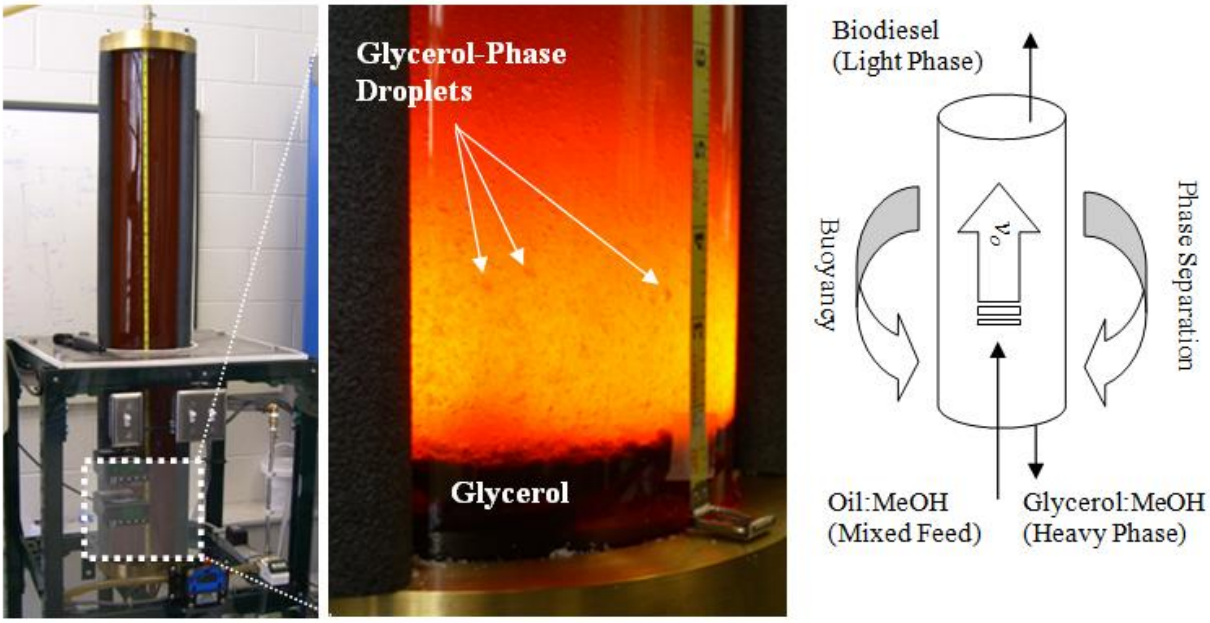

Figure 1: Biodiesel Continuous Flow Reactor showing glycerol droplets separating from oil phase (left) and overall phase separation of products (right).

The biodiesel reaction is a heterogeneous two-phase reaction where the biodiesel phase readily separates from the glycerol phase. During laboratory experiments, glycerol droplets could be readily seen separating from the bulk flow and falling to the bottom of the reactor. Described by Boucher, the settling velocity of glycerol droplets through an oil phase (biodiesel, oil) is proportional to the difference in densities of the two phases, the droplet size of the settling phase (glycerol), and the viscosity of the continuous phase (oil and biodiesel) [8]. In the up-flowing oil phase, molecules of glycerol are created by reaction. The glycerol molecules nucleate into small droplets, most likely via a heterogeneous mechanism due to very small particulate contamination in the vegetable oil as well as hydrophobic interactions. The small droplets initially flow upward with the oil phase since their settling velocity downward is much smaller than the upward velocity of the oil phase. The small droplets coalesce with each other to form larger droplets, and when they reach sufficient size they begin falling downward as the settling velocity becomes larger than the upward oil velocity. In the actual operation, the partitioning of methanol and catalyst has an effect on the nucleation, coalescence and settling time of glycerol droplets. Methanol partitioning between the glycerol and oil phase affects the densities and viscosities of each phase and the size of the glycerol droplets. The reaction rate will be affected by the partitioning of methanol and catalyst.

D. Modeling Approaches

Modeling of the Biodiesel Reactor deals with many challenges, including chemical reaction of liquid-liquid systems, phase separation of products, complex two-phase flow, and mass transfer from reaction and diffusion. Michael Lines, a Master's student at the University of Connecticut, proposed a pseudo-homogenous model to predict overall reactor performance [7]. A standard plug flow reactor model with axial dispersion was initially theorized, but the results failed to predict experimental conversions or any phase separation, which indicated that capturing phase separation was necessary to predicting reactor performance. The plug flow reactor model was modified by removing the axial

dispersion term and including a velocity term for each species due to buoyance forces. Both model were implemented and solved in Matlab. The results of the modified plug flow reactor captured the phase separation and exit flows from the top and bottom of the reactor, and predicted the trend toward higher conversions throughout the length of the reactor.

Following Lines's work, Brian Chakulski focused his Master's thesis on using different approaches for modeling multiphase reacting systems [9]. Chakulsi was guided by Dr. Frederick Phelan of NIST, and developed a method that used Cahn-Hilliard theory to understand the complicated transport phenomena in the reacting mixture. The Cahn-Hilliard theory assumes that diffusion is driven by the gradient of chemical potential, and other free energy models besides the traditional Double Well potential used in Cahn-Hilliard. Navier-Stokes equations were used to model flow dynamics. The model was solved in COMSOL Multiphysics to utilize the time-dependent differential equation solver. The biodiesel reacting mixture was simplified into binary solution of biodiesel and glycerol because the authors intended to derive an accurate model of the phase separation occurring in the reactor. The first attempt to model the binary system did not achieve separation because of ideal solution assumptions. With the regular solution theory, the results showed separation of the binary mixture into two phases. The reacting mixture was extended into a quaternary component mixture, to increasing similarity to the biodiesel system, but attempts with this model were not successful because of limiting computer processing power.

The objective of this paper was to improve on Chakulski's model, under the guidance Dr. Phelan. The separation of an initially homogenous, ternary mixture (Biodiesel, methanol, and glycerol) was shown to separate into two phases. The partitioning of methanol between the organic and aqueous phase was described by a ternary free energy expression. From liquid-liquid equilibrium data of the ternary system, applicable parameters were found which would allow the separation components to be

at equilibrium concentrations. A gravity component to the Navier-Stokes equations was added, and it was discovered that COMSOL solver could not handle the scaling problems. To resolve the issue, a dimensionless form of the model was adopted. This approach would make computation easier for the solver, and indeed many literature sources used dimensionless models when solving phase separation problems.

II. Model System

In the development of a phase separation model for the biodiesel reacting system, it was necessary to apply phase field theory, a class of diffuse-interface models. One of the applications for which phase field models are particularly well-suited is the complex process of phase separation, structure formation and evolution in flow systems, an area of technological impact in soft materials processing. This basic idea of this method is to introduce an order parameter or phase field that varies continuously over thin interfacial layers and is mostly uniform in the bulk phases. A well known phase field model is the Cahn-Hilliard equation, which is used for modeling phase separation in a binary mixture quenched into an unstable region. The relaxation of the order parameter is driven by a local minimization of the free energy subject to phase field conservation and as a result, interface layers do not deteriorate dynamically [10]. The fluid dynamics can be applied by coupling the convective Cahn-Hilliard equation with Navier-Stokes equations.

A. Phase field method

Phase field methods allow us to account for interfaces with nonzero thickness. It is assumed that the state of the system at any given time can be described by an order parameter *c* which is a function of the position vector. In this work, we consider a ternary system consisting of three species: biodiesel, methanol, and glycerol. Let $c_i(\mathbf{r},t)$ for *i*=biodiesel, methanol, and glycerol represent the mole fraction of the *i*th component as a function of position **r** and time *t*. Since c_i is a mole fraction, we have the following condition

$$c_1 + c_2 + c_3 = 1 \tag{1}$$

Three free energy of mixing formulations have been proposed for the ternary system. Dr. Phelan provided the first formulation, based on the double well potential. The double well potential, commonly used in Cahn-Hilliard formulations, provides a means for calculating an analytical phase separation [9]. In terms of mole fractions, the double-well potential is written as [11],

$$g(c_1, c_2, \dots, c_n) = 4\sum_{i=1}^{n}\sum_{j=1+i}^{n} c_i^2 c_j^2 \quad (2)$$

For ternary systems, the double well potential is written as

$$g(c_1, c_2, c_3) = 4(c_1^2 c_2^2 + c_1^2 c_3^2 + c_2^2 c_3^2) \quad (3)$$

The double-well potential may be generalized as

$$g(c_1, c_2, c_3) = a c_1^2 c_2^2 + b c_1^2 c_3^2 + d c_2^2 c_3^2 \quad (4)$$

Where $c_3 = 1 - c_1 - c_2$ and *a*, *b*, and *d* are constants and equal to 4. **Figure 2** is the surface plot of the double well potential on the Gibbs triangle, created by Dr. Phelan. Three minimums in *g* are exhibited, which form three equilibrium phases corresponding to the pure components. Changing the constants does not shift the corners of the phase diagram. This formulation is not applicable to our system because rather than forming three separate phases, methanol partitions between the biodiesel and glycerol phases.

Kim *et al.* provides an approximation for the free energy of a three-component system, which serves to be the second formulation used in this ternary system [12]. The expression reads:

$$g(c_1, c_2, x_3) = a c_1^2 c_2^2 + b(c_1^2 + c_2^2) c_3^2 - d c_1 c_2 c_3 \quad (5)$$

When the *a*, *b*, and *d* constants are equal to ¼, the surface plot of the free-energy for the ternary system presents minima in the corners of the diagram and at the center of it, where the system is fully miscible (see **Figure 3**, created by Dr. Phelan).

Tufano *et al.* observed that after changing the parameters in Eq. 5, the free-energy surface plot remains symmetrical around one of the axes [13]. Therefore, this formulation is not applicable, because

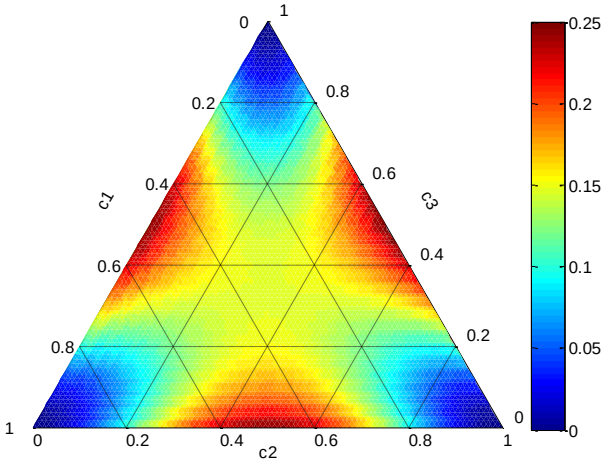

Figure 2: Surface plot of the double well potential (Eq. 4) on the Gibbs triangle for a=b=d=4.

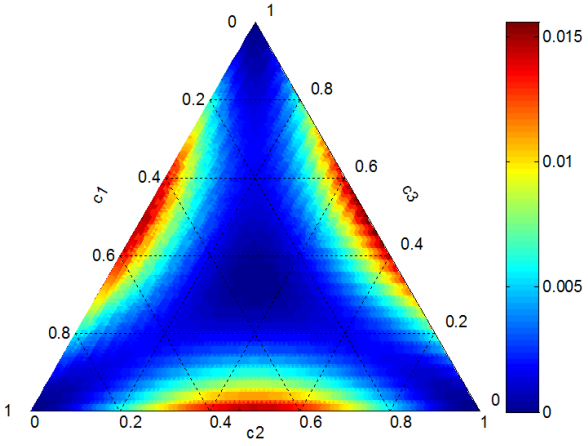

Figure 3: Surface plot of the free energy (Eq. 5) on the Gibbs triangle for a=b=d=1/4.

a fourth phase is not formed, and another free-energy formulation is required.

An alternative free-energy formulation for ternary partially miscible systems proposed by Kim and Lowengrub is used [14],

$$g(c_1, c_2, c_3) = ac_1^2c_3^2 + (c_1 + b)(c_2 - d)^2 + (e - c_1 - c_2)(c_2 - f)^2 \quad (6)$$

Using constants of *a*=2, *b*=0.2, *d*=0.2, *e*=1.2, and *f*=1.04, the surface and contour plots of this free-energy formulation are shown in **Figure 4**, created by Dr. Phelan. The contour plot corresponding to Eq. 6 shows two minimums in *g*, where two equilibrium phases are formed in which c_2 is miscible in both c_1 and c_3. This is suitable to describe our three-component system.

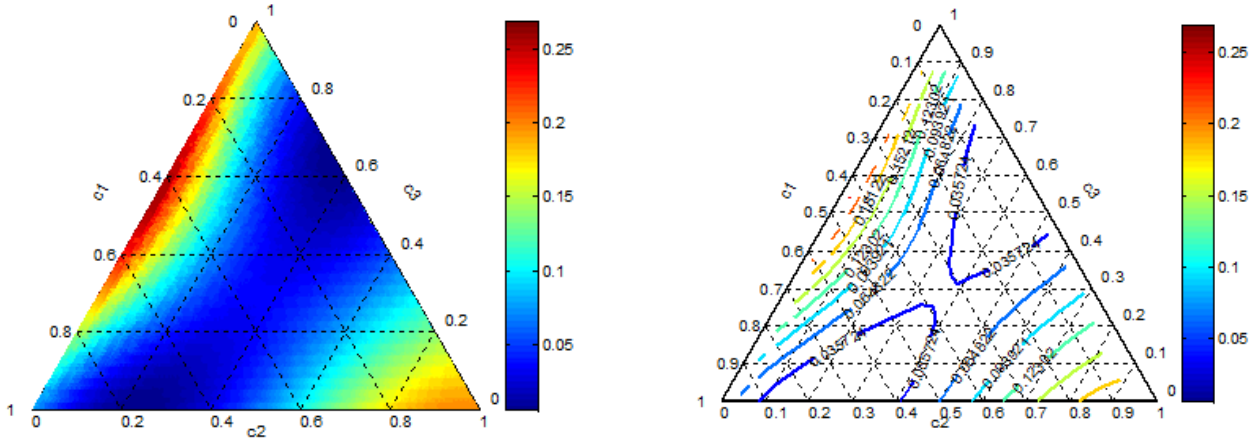

Figure 4: Surface plot (left) and contour plot (right) of the free-energy (Eq. 6) on the Gibbs triangle for *a*=2, *b*=0.2, *d*=0.2, *e*=1.2, and *f*=1.04.

A generalized chemical potential based on the free-energy formulations is defined as [15]

$$\mu_i = \left(\frac{\delta nG}{\delta c_i}\right)_{T,P,n_1,\ldots,n_{k\neq i}} \quad (7)$$

Where *G* is the total free energy, $n=n_1 + n_2 + \ldots$ represents the moles of various components and the $\frac{\delta}{\delta x}$ operator denotes the variational partial derivative defined as

(8)

$$\frac{\delta f}{\delta x} = \frac{\partial f}{\partial x} - \nabla \cdot \frac{\partial f}{\partial(\nabla x)}$$

By satisfying Euler's theorem and Gibbs-Duhem equation, the chemical potential for a particular component can be expressed as [15]

$$\mu_i = G + (1 - c_i)\left(\frac{\delta G}{\delta c_i}\right)_{c_1,\ldots,c_{k\neq i}} - \sum_{j\neq i} c_j \left(\frac{\delta G}{\delta c_i}\right)_{c_1,\ldots,c_{k\neq j}} \quad (9)$$

Where $\left(\frac{\delta G}{\delta c_i}\right)_{c_1,\ldots,c_{k\neq i}}$ are the variational derivatives of *g* given by

$$\left(\frac{\delta G}{\delta c_i}\right)_{c_1,\ldots,c_{k\neq i}} = \left(\frac{\partial G}{\partial c_i}\right)_{\substack{c_1,\ldots,c_{k\neq i}\ldots,c_n;\\ \nabla c_1,\ldots,\nabla c_n}} - \left(\frac{\partial G}{\partial \nabla c_i}\right)_{\substack{c_1,\ldots,c_n;\\ \nabla c_1,\ldots\nabla c_{k\neq i}\ldots,\nabla c_n}} \quad (10)$$

A proportional flux method proposed by Alfarraj and Nauman is chosen to evaluate the chemical potential [16]. This method was tested using molecular dynamics for the diffusion of short-chain alkanes and can be applied to the phase separation by spinodal decomposition in ternary, asymmetric systems of polymers and solvents. The variational free energy is given by:

$$\left(\frac{\delta G}{\delta c_1}\right)_{c_2,c_3} = \frac{\partial g}{\partial c_1} - \kappa_1 \nabla^2 c_1 - \kappa_3 \nabla^2 c_2 \quad (11)$$

$$\left(\frac{\delta G}{\delta c_2}\right)_{c_1,c_3} = \frac{\partial g}{\partial c_2} - \kappa_3 \nabla^2 c_1 - \kappa_2 \nabla^2 c_2 \quad (12)$$

$$\left(\frac{\delta G}{\delta c_3}\right)_{c_1,c_2} = \frac{\partial g}{\partial c_3} \quad (13)$$

where κ_i's are the gradient energy parameters. The gradient energy parameters are known to be functions of the radius of gyration and the interaction parameters. However, those are relevant to polymeric systems to describe the enthalpic and entropic effects [17]. To describe our system of

comparably smaller molecules, theoretical derivations of these parameters are currently unknown. Thus, they were assumed to be 0.001 (a guess value), and candidates for parameter estimation.

The equilibrium interface profile can be found by minimizing the total free energy *G* with respect to variations of the function *c*, or in other words solving for μ(*c*). Cahn and Hilliard generalized the problem to time-dependent situations by approximating interfacial diffusion fluxes as being proportional to chemical potential gradients, enforcing conservation of the field. The diffusional flux may be written as,

$$j_i = D_i \nabla \mu_i \tag{14}$$

where D_i is the diffusion coefficient of component *i* and terms involving cross diffusion have been ignored. Based on these assumptions, the conservation equation for each species is expressed as,

$$\frac{\partial c_i}{\partial t} + u \cdot \nabla c_i = \nabla \cdot (D_i \nabla \mu_i) \tag{15}$$

where *u* is the velocity field. Eq. 15 models the creation, evolution, and dissolution of diffusivity controlled phase field interfaces [18]. At the wall, we adopt the following no-flux boundary conditions:

$$n \cdot \nabla c_i = 0 \; and \; n \cdot D_i \nabla \mu_i = 0 \tag{16}$$

where *n* is the unit vector normal to the domain boundary.

B. The equations of motion

The three-component fluid flow is considered viscous and incompressible. The fluid dynamics are described by the Navier-Stokes equations.

$$\rho\left(\frac{\partial u}{\partial t} + u \cdot \nabla u\right) = -\nabla p + \nabla \cdot \eta(\nabla u + \nabla u)^T + \rho(\mu_1 \nabla c_1 + \mu_2 \nabla c_2) \tag{17}$$

$$\nabla \cdot u = 0 \tag{18}$$

where u is the velocity field, p is the scalar related to the pressure that enforces the incompressiblity constraint, and η is the viscosity. The superscript T stands for the transpose operator. At a wall the Dirichlet boundary condition is imposed for the velocity field, or $u=u_o$ at a fixed domain boundary [10].

The coupled Cahn-Hilliard/Navier-Stokes system (Eq. 15-18) is refered to as "Model H" according to the nomenclature of Hohenburg and Halperin [19].

C. Interface properties

The binary case is considered applicable to describe the three-component system because two-phases are exhibited. The diffuse-interface model uses a specific form of the Helmholtz free energy function based on the approach by Cahn and Hilliard in 1958. The free energy of a binary fluid can be expressed as [10],

$$G(c,\nabla c) = g(c) + \frac{1}{2}\kappa\,|\nabla c|^2 \tag{19}$$

Where g is the homogenous part of the specifc free energy and κ is the gradient energy parameter. The homogenous part g shown below is approximated by the Landau-Ginzburg free energy [20]:

$$g(c) = \frac{1}{4}\beta c^4 - \frac{1}{2}\alpha c^2 \tag{20}$$

Another formluation is called the Double Well potential is [10],

$$g(c) = \frac{\alpha}{4}\left(c - \sqrt{\frac{\beta}{\alpha}}\right)^2\left(c + \sqrt{\frac{\beta}{\alpha}}\right)^2 \tag{21}$$

where α and β are constants. The equilibrium profile is given by the solutions of the equation

$$\mu(c) = \frac{\delta G}{\delta c} = \alpha c^3 - \beta c - \kappa\nabla^2 c = 0 \tag{22}$$

This leads to the equilibrium bulk concentrations in the segregated bulk phases,

$$c_B = \sqrt{\frac{\kappa}{\alpha}} \tag{23}$$

and a one-dimensional (for example along the z-direction) non-uniform solution

$$c_o(z) = c_B \tanh\left(\frac{z}{\sqrt{2}\xi}\right) \tag{24}$$

that satisfies the boundary conditions $c_o(z \to \infty) = \pm c$. This solution describes the equilibrium profile for a plane interface normal to the z-direction, of thickness proportional to

$$\xi = \sqrt{\frac{\kappa}{\beta}} \tag{25}$$

that separates the two bulk phases.

In equilibrium the surface tension of an interface is equal to the integral of the free energy density along the interface. For a planar interface, the surface tension is given by [21]

$$\sigma = \frac{\sqrt{2}}{3}\kappa^{\frac{1}{2}}\frac{\beta^{\frac{1}{2}}}{\alpha} \tag{26}$$

If α is assumed to equal to κ (gradient energy parameter) and β can be written in terms of surface tension and interface thickness [22],

$$\kappa = \frac{3}{\sqrt{2}}\sigma\xi \;\; and \;\; \beta = \frac{3}{\sqrt{2}}\frac{\sigma}{\xi} \tag{27}$$

D. Non-dimensionalization

The governing equations are non-dimensionalized using the dimensionless variables [20]:

$$\hat{c} = \frac{c}{c_B} \qquad \hat{t} = \frac{tU}{L} \qquad \hat{g} = \frac{g\xi^2}{\kappa c_B^2}$$

$$\hat{u} = \frac{u}{U} \qquad \hat{\mu} = \mu\frac{\xi^2}{\kappa c_B} \qquad \hat{\eta} = \frac{\eta}{\eta_1}$$

$$\hat{\nabla} = L\nabla \qquad \hat{p} = \frac{pL}{\eta_1 U}$$

The characteristic scale U is the maximum value of *u*. For the characteristic length *L* either the domain length or interface thickness can be used, and in our case, the domain length is used.

The system of equations reads[1], (after dropping the asterisks and assuming no bulk flow)

$$Re * \rho\frac{d}{dt}(u) = -\nabla \mathrm{p} + \eta\nabla^2 u + \frac{\rho_1 c_B}{CaC_h} * \rho * (\mu_1\nabla c_1 + \mu_2\nabla c_2) \tag{28}$$

$$\frac{d}{dt}(c_1) + u\cdot\nabla(c_1) = \frac{1}{Pe}\nabla\cdot(\nabla\mu_1) \tag{29}$$

$$\frac{d}{dt}(c_2) + u\cdot\nabla(c_2) = \frac{1}{Pe}\nabla\cdot(\nabla\mu_2) \tag{30}$$

$$\mu_1 = \left[\frac{\partial g}{\partial c_1}\right] - c_h^2\nabla^2(c_1) \tag{31}$$

$$\mu_2 = \left[\frac{\partial g}{\partial c_2}\right] - c_h^2\nabla^2(c_2) \tag{32}$$

The dimensionless groups that appear are: Peclet number *Pe*, capillary number *Ca*, Cahn number C_h, and Reynolds number *Re*.

$$Pe = \frac{UL\xi^2}{D\kappa} \qquad C_h = \frac{\xi}{L}$$

$$C_a = \frac{\eta_1 U\xi}{\kappa c_B} \qquad Re = \frac{\rho_1 U^2}{L}$$

[1] Refer to the Derivations section in the Appendix for precise understanding of the governing equations

The density and viscosity functions are estimated by a linear function given by

$$\rho = \sum_{i=1}^{N} \rho_i x_i \tag{32}$$

$$\eta = \sum_{i=1}^{N} \eta_i x_i \tag{33}$$

where x_i is the mass fraction of the *i*th-component.

III. Results

The appropriate reactant mixture contains six moles of methanol for every mole of triglyceride. Here we attempt to model the phase separation of the final mixture assuming 100% conversion, where the mixture should contain 3:3:1 molar ratios of biodiesel to methanol to glycerol. The initial mole fraction of biodiesel (c1_initial) is 0.43 and of methanol (c2_initial) is 0.43. The initial concentration values are described by the following functions to model an initially mixed system with concentration fluctuations,

c1_initial+0.01*sin(16*pi*x)*sin(16*pi*y)

c2_initial+0.01*sin(16*pi*x)*sin(16*pi*y)

The phase separation model is solved in COMSOL Multiphysics 4.0a. The solution procedure is as follows:

- Solve for (v,p) using the Navier-Stokes module
- Solve for (c, μ) in the built-in COMSOL partial differential equation (PDE) module

The documentation of the COMSOL file that is discussed in this paper can be found in the Appendix section.

The layout of the Results section begins with Model 1, the solution to previously described model equations (Eq. 28-32). The model equations are altered with addition terms to the chemical potential formulations, called Model 2. Model 2 has higher complexity than Model 1, and their phase separation outcomes differ due to the alteration.

A. Model 1

The governing equations of Model 1 are listed in Eqs. 28-32. The COMSOL results for the characteristic time range of 0 to 4 are shown below. The contour plot, whose magnitude is indicated by the color bar to the far right, refers to the concentration of component 1 (biodiesel). The line plot

represents the concentration of component 3 (glycerol). Component 2 (methanol) is not shown in the graphs, but can be determined with knowledge of components 1 and 3. The arrows indicate the velocity in x- and y- directions.

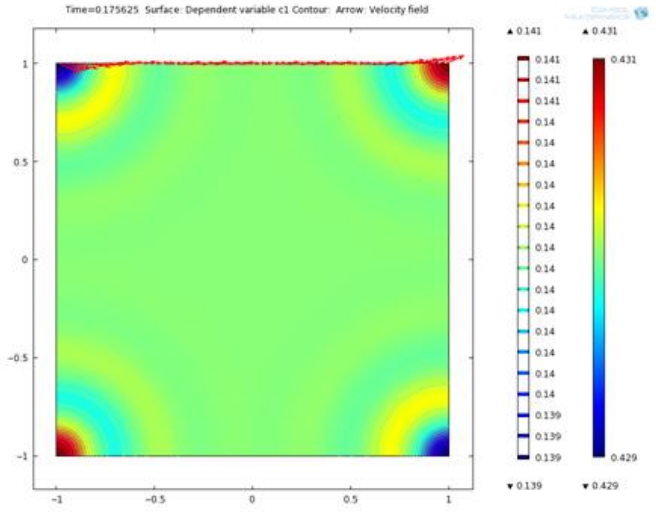

Figure III-1: Time = 0.18

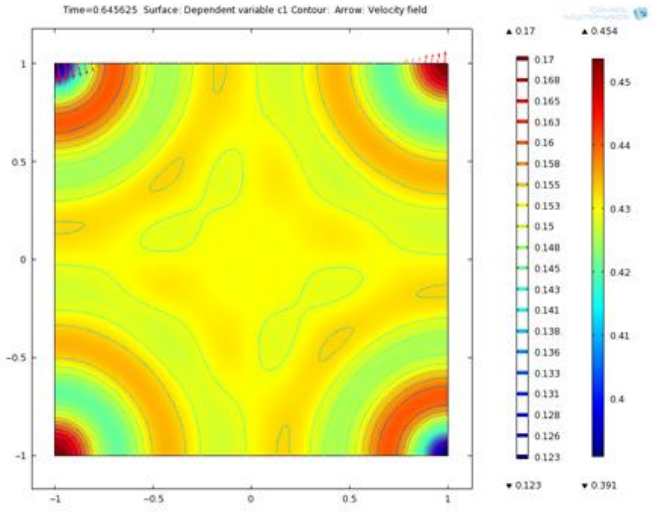

Figure III-2: Time = 0.65

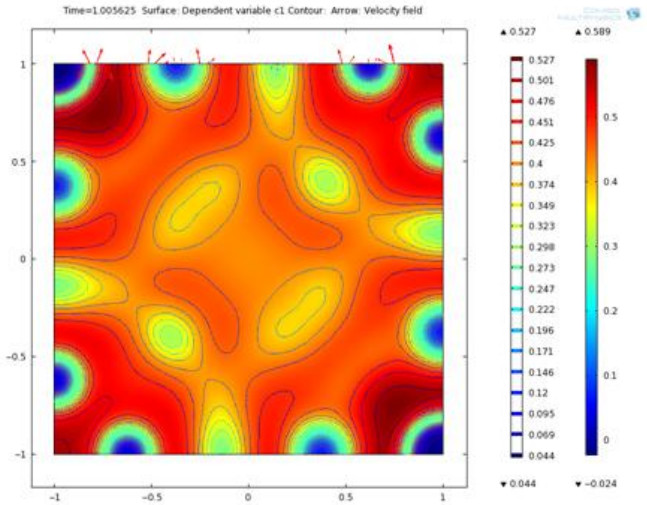

Figure III-3: Time = 1.00

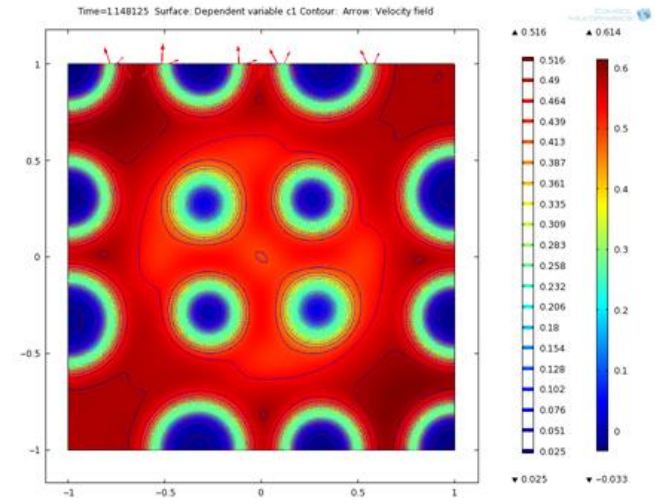

Figure III-4: Time = 1.15

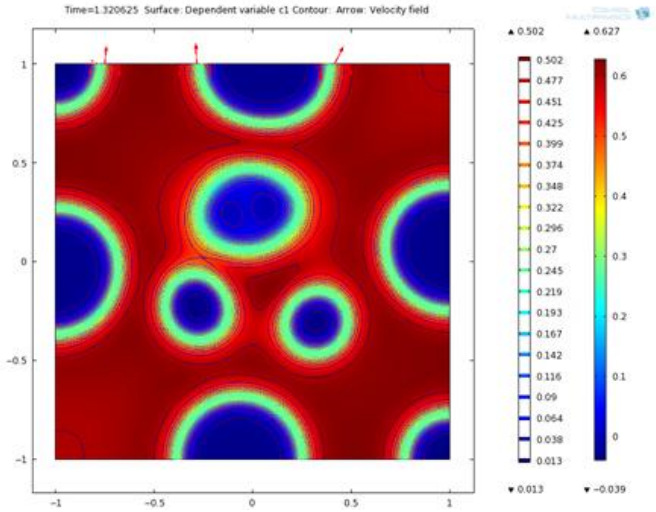

Figure III-5: Time = 1.32

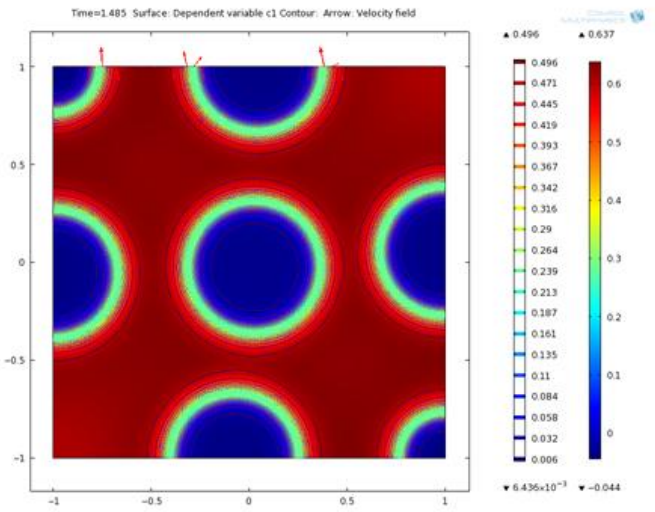

Figure III-6: Time = 1.48

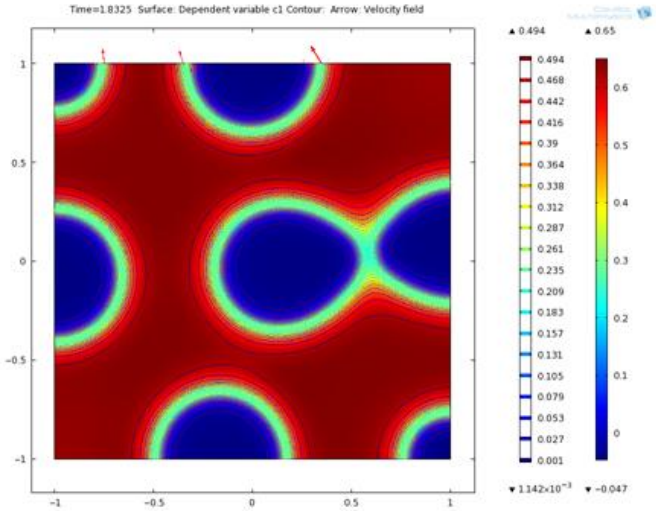

Figure III-7: Time = 1.83

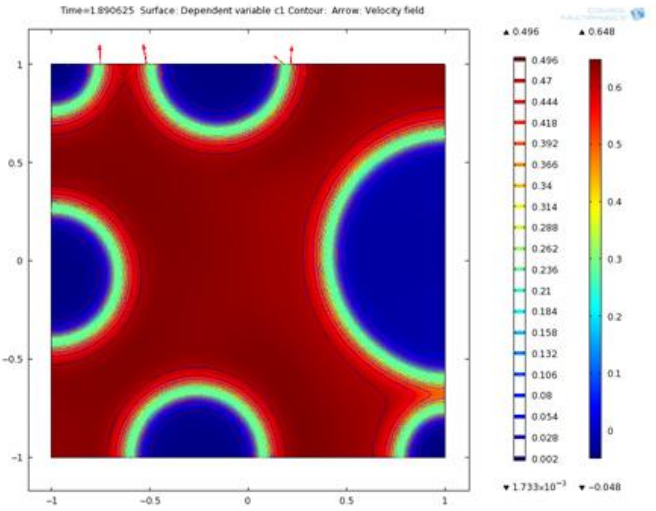

Figure III-8: Time = 1.89

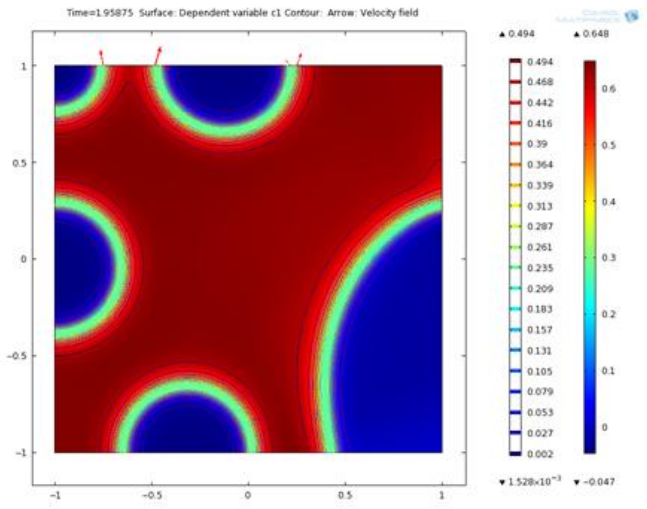

Figure III-9: Time = 1.96

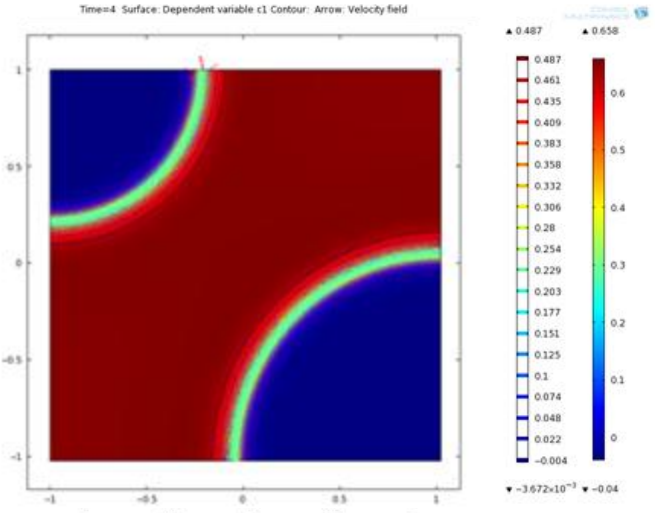

Figure III-10: Time = 4

B. Model 2

The adjusted chemical potential formulations of Model 2 are seen below (Eqs. 34, 35). All other governing equations from Model 1 are consistent in Model 2. This is formulation is actually more similar to the variational free energy proposed by Alfarraj and Nauman [16]. The proposed chemical potential is related to the gradient of the total free energy variational partial derivative. The simplification made here eliminates the gradient operator, and thus relates chemical potential to the free energy variational partial. The derivations of Model and 2 are located in the Appendix of this text. Without simplification, it will be challenging to calculate the exact chemical potential functions in COMSOL. Furthermore, this simplification is recommended by Dr. Phelan for the purposes of this work, but for future work, it is recommended that exact formulations be used instead. The COMSOL results for Model 2 are shown below. Again, the contour plot refers to biodiesel, line plot refers to glycerol, and the arrows refer to the field components.

$$\mu_1 = \left[\frac{\partial g}{\partial c_1}\right] - c_h^2\nabla^2(c_1) - c_h^2\nabla^2(c_2) \tag{34}$$

$$\mu_2 = \left[\frac{\partial g}{\partial c_2}\right] - c_h^2\nabla^2(c_1) - c_h^2\nabla^2(c_2) \tag{35}$$

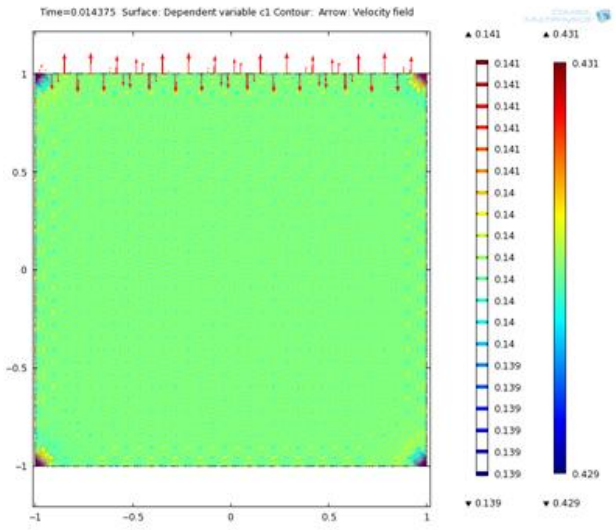

Figure III-11: Time = 0.01

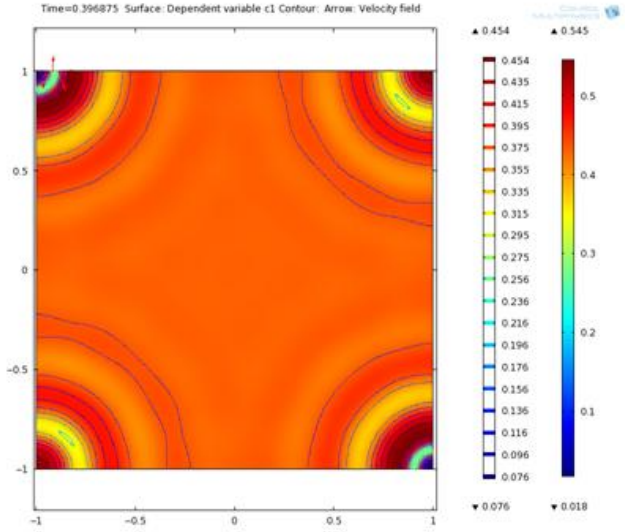

Figure III-12: Time = 0.40

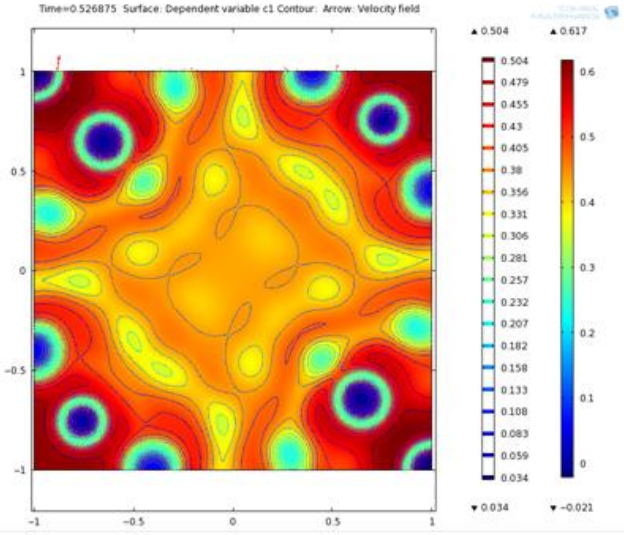

Figure III-13: Time = 0.53

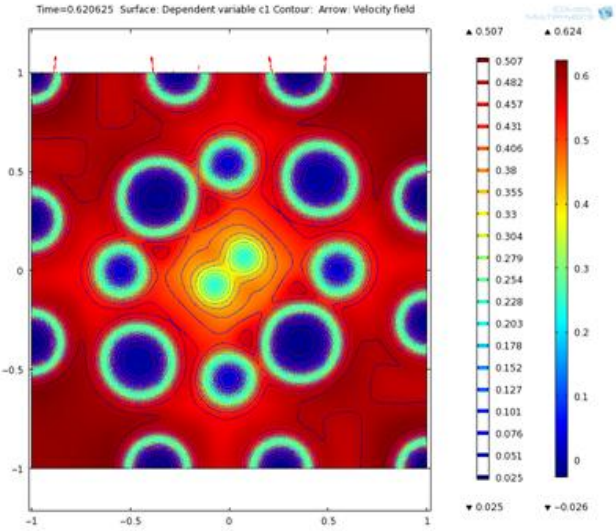

Figure III-14: Time = 0.62

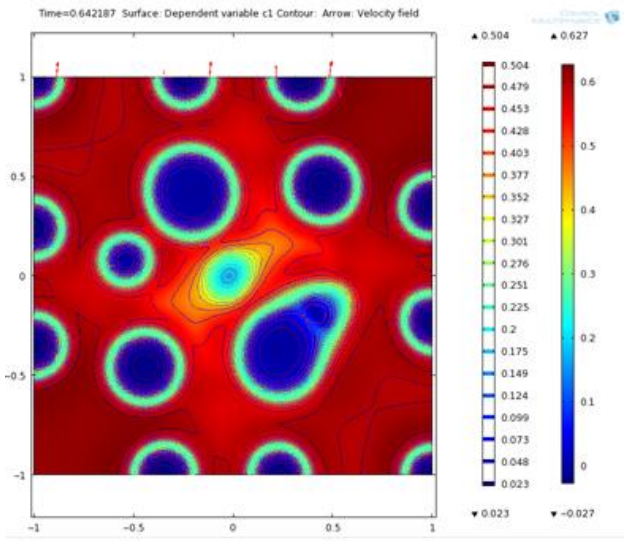

Figure III-15: Time = 0.64

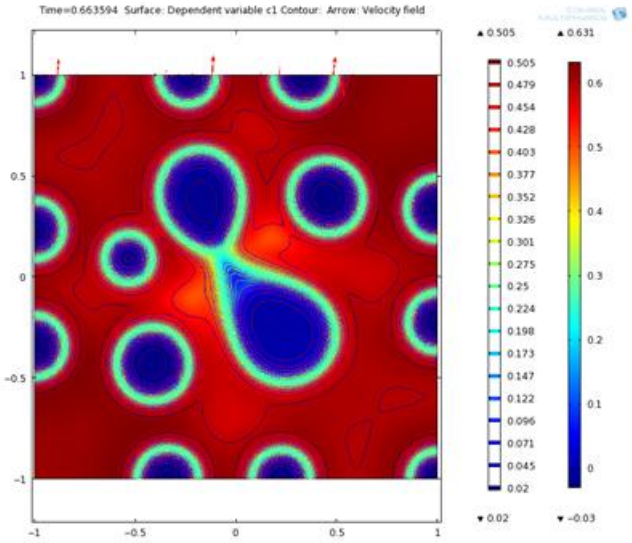

Figure III-16: Time = 0.66

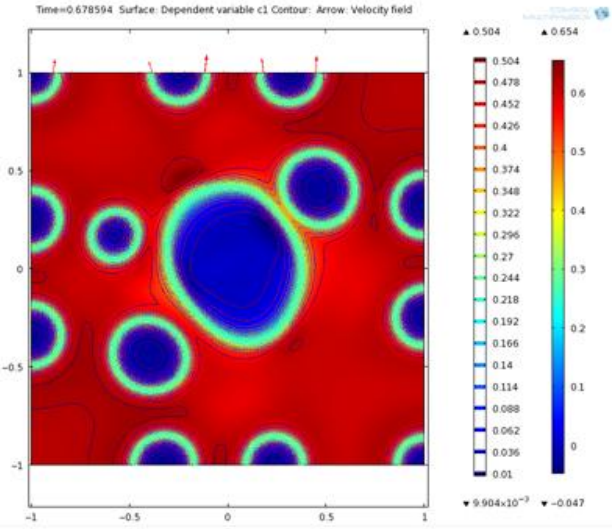

Figure III-17: Time = 0.68

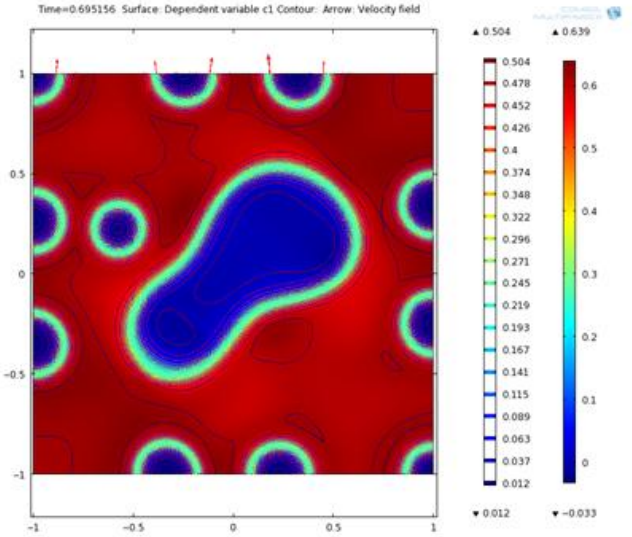

Figure III-18: Time = 70

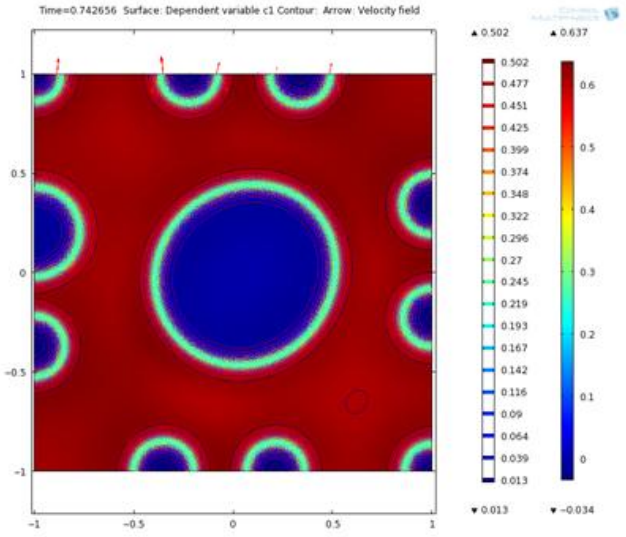

Figure III-19: Time = 0.74

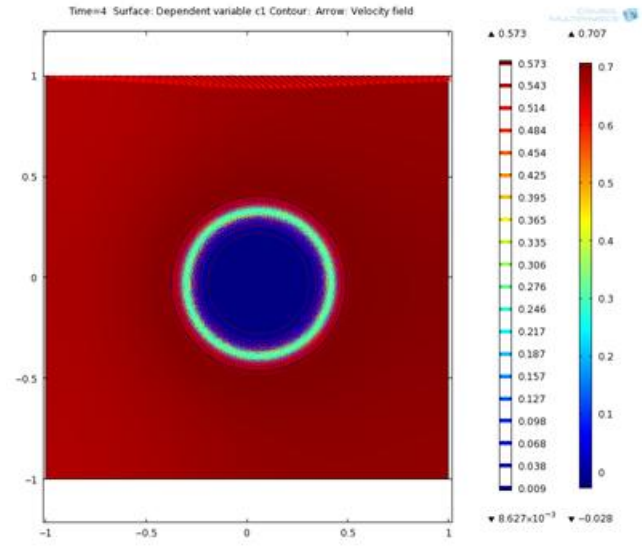

Figure III-20: Time = 4

The differences observed in phase separation behavior between Models 1 and 2 can be only contributed to the chemical potential formulations. At the final characteristic time, Model 1 does not observe complete phase separation behavior, as the phase containing methanol and glycerol appears at upper-left and lower-right corners. In Model 2, the same phase forms one "bubble" at the center of the diagram. A stronger nucleation force is exhibited in Model 2 because the components have a stronger tendency to coalesce into two distinct phases. Note that gravity force is not included in Models 1 and 2, but the results with gravity are shown in the Appendix section.

C. Bulk equilibrium concentrations

Given the free energy formulation and parameters suggested by ref [14], the organic and aqueous phases exhibit the concentrations listed in **Table 1**. If the COMSOL models are solved for a larger time range, then the bulk concentrations will eventually approach the equilibrium values.

	Oil phase	Aqueous phase
Biodiesel	0.78	≈0
Methanol	0.23	0.37
Glycerol	≈0	0.65

Table 1: Bulk concentrations*

It is unknown to the author what the realistic bulk concentrations are for the biodiesel system under the initial conditions. In the future, an experimental procedure will need to determine actual concentrations of the two phases. If the values are soon to be known to future authors, then it is recommended to adjust the free energy parameters for the minimum loci to reside over the realistic values. Preliminary attempts have shown that the bulk concentrations also depend on the initial concentrations.

*Although minimization of free energy results in negative terms, the smallest physical concentration is zero

IV. Conclusions

This approach using Cahn-Hilliard theory showed that phase modeling can be applied to biodiesel systems. It is illustrated that a ternary system will separate into two phases with the recommended free energy expression. Interfacial properties and their dependents have been used to capture the real interface. The governing equations are scaled accordingly by introducing dimensionless numbers. A key finding is that although the chemical potentials have been simplified, the formulation from Model 2 shows greater capability to model nucleation.

The major contribution to Brian Chakulski's previous work is that this model extends the binary system by another component. The double well potential for a three-component system has proven to be unable to capture partial miscibility, as exhibited from the partitioning of methanol between the biodiesel and glycerol phases. Instead, an alternative formulation is used because the minimization of free energy allows the two equilibrium phases to be formed, with one miscible component appearing in both. Furthermore, the applicability to a regular solution has been greatly extended, with interfacial relationships, realistic initial conditions, cited chemical potentials, and scaling definition.

V. Discussion

The limitations include the estimation of key parameters, including the diffusion coefficients, gradient energy parameters, and double well potential constants. New parameters in the free energy formulation will be needed to characterize the actual bulk concentrations. The overall biodiesel system is truncated to only three components, and chemical reaction is neglected. Bulk flow is also ignored, in favor of a stationary system. Even with these limitations, this paper demonstrates that it is possible to formulate a phase separation model for Biodiesel systems.

VI. Appendix

A. Model 1 with gravity

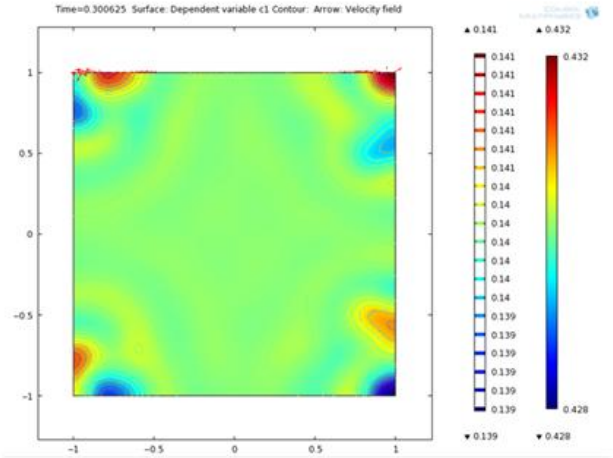

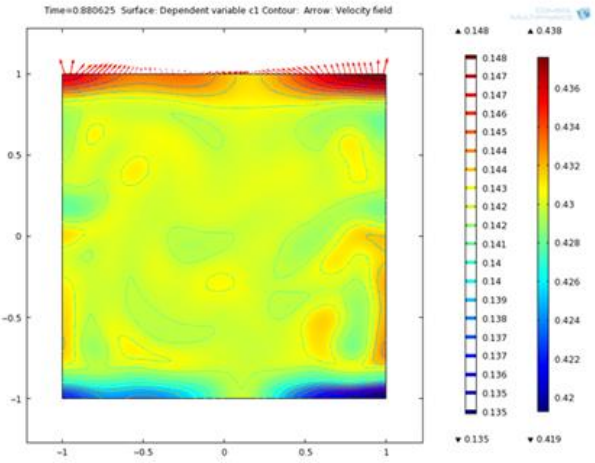

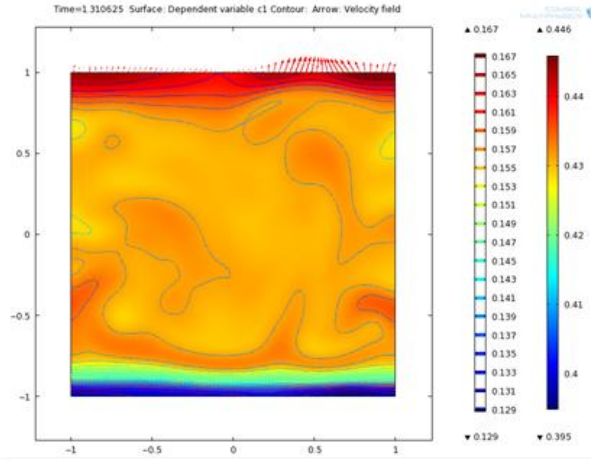

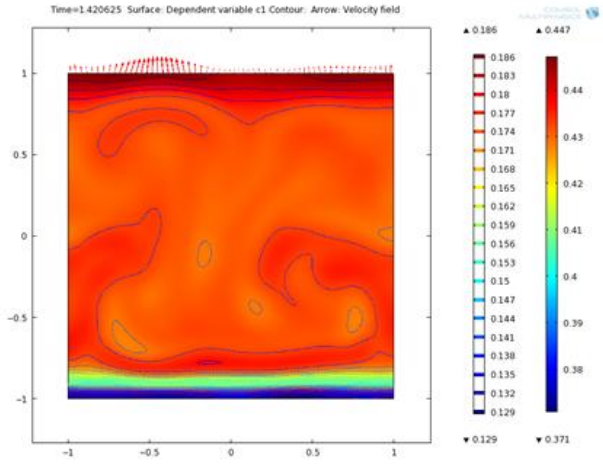

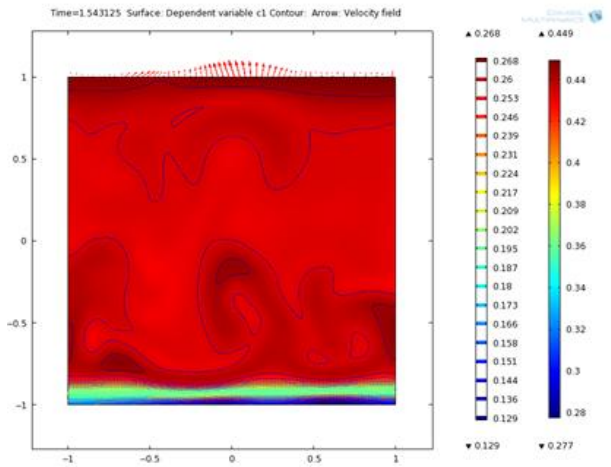

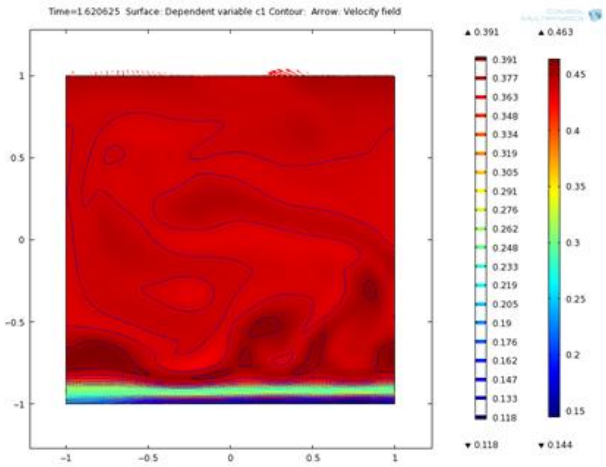

B. Model 2 with gravity

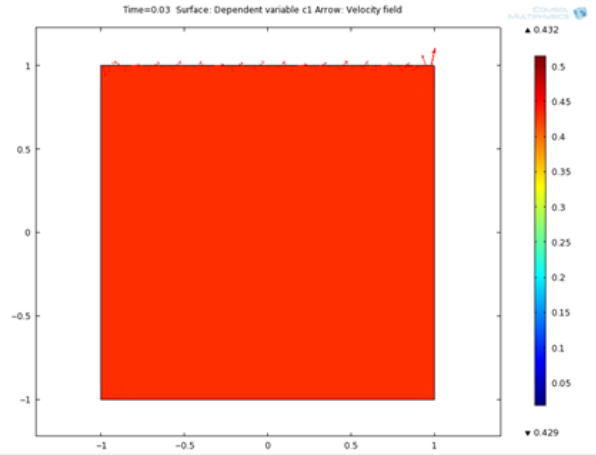

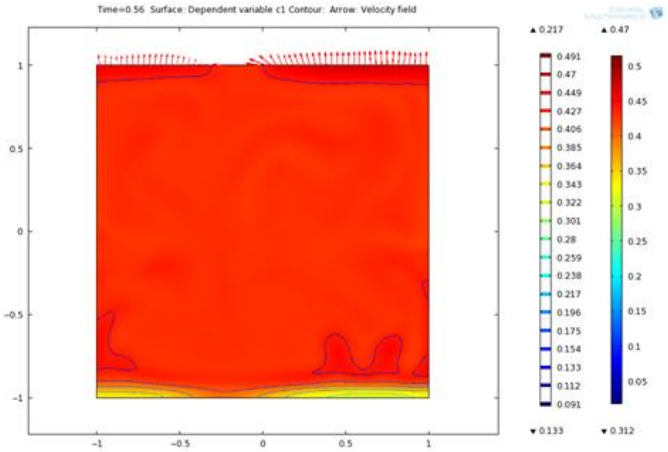

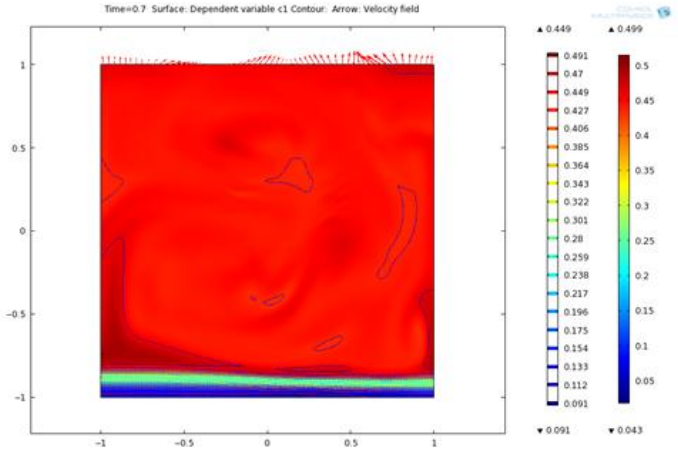

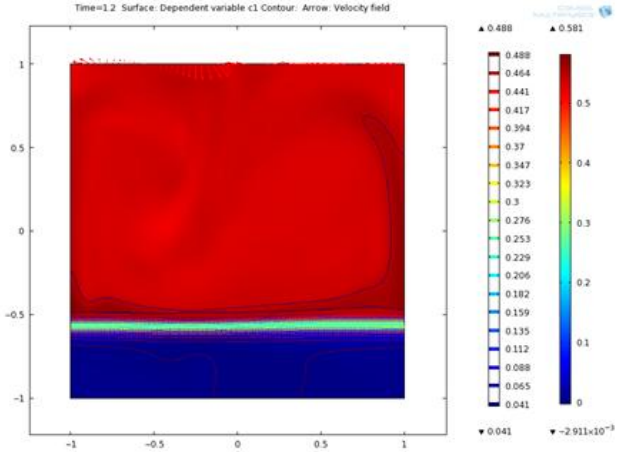

C. Derivations

1. Scaling Navier-Stokes equations (with gravity term)

$$\rho\frac{du}{dt} = -\nabla p + \eta\nabla^2 u + \rho(\mu_1\nabla c_1 + \mu_2\nabla c_2) + \rho g$$

$$\frac{\rho_1 U^2}{L}\hat{\rho}\frac{d}{d\hat{t}}(\hat{u}) = -\left(\frac{\eta_1 U}{L^2}\right)\hat{\nabla}\hat{p} + \left(\frac{\eta_1 U}{L^2}\right)(\hat{\eta}\hat{\nabla}^2\hat{u}) + \left(\frac{\rho_1\kappa c_B}{\xi^2 L}\right)\left[\hat{\rho}\left(\hat{\mu}_1\hat{\nabla}\hat{c}_1 + \hat{\mu}_2\hat{\nabla}\hat{c}_2\right)\right] + \hat{\rho}\rho_1 g$$

$$\left(\frac{\rho_1 U^2}{L}\right)\left(\frac{L^2}{\eta_1 U}\right)\hat{\rho}\frac{d}{d\hat{t}}(\hat{u}) = -\hat{\nabla}\hat{p} + \left(\hat{\eta}\hat{\nabla}^2\hat{u}\right) + \frac{\rho_1 c_B}{CaC_h} * \hat{\rho} * \left(\hat{\mu}_1\hat{\nabla}\hat{c}_1 + \hat{\mu}_2\hat{\nabla}\hat{c}_2\right) + \left(\frac{\rho_1 L^2}{\eta_1 U}\right)\hat{\rho} g$$

$$Re * \hat{\rho}\frac{d}{d\hat{t}}(\hat{u}) = -\hat{\nabla}\hat{p} + \left(\hat{\eta}\hat{\nabla}^2\hat{u}\right) + \frac{\rho_1 c_B}{CaC_h} * \hat{\rho} * \left(\hat{\mu}_1\hat{\nabla}\hat{c}_1 + \hat{\mu}_2\hat{\nabla}\hat{c}_2\right) + \left(\frac{\rho_1 L^2}{\eta_1 U}\right)\hat{\rho} g$$

2. Scaling continuity equation

$$\frac{d}{dt}(c_1) + u\cdot\nabla(c_1) = \nabla\cdot(D\nabla\mu_1)$$

$$\frac{Uc_B}{L}\left[\frac{d}{d\hat{t}}(\hat{c}_1) + \hat{u}\cdot\hat{\nabla}(\hat{c}_1)\right] = \frac{\hat{\nabla}^2}{L^2}\frac{D\hat{u}_1\kappa c_B}{\xi^2}$$

$$\frac{d}{d\hat{t}}(\hat{c}_1) + \hat{u}\cdot\hat{\nabla}(\hat{c}_1) = \frac{D\kappa}{U\xi^2 L}\hat{\nabla}^2\hat{u}_1$$

$$\frac{d}{d\hat{t}}(\hat{c}_1) + \hat{u}\cdot\hat{\nabla}(\hat{c}_1) = \frac{1}{Pe}\hat{\nabla}^2\hat{u}_1$$

3. Scaling of chemical potential equation

As advised by Dr. Phelan, the free energy expression by Alfarraj and Nauman was initially simplified into(note: c_3 is not specified because c_3=1-c_1-c_2 and g is only a function of c_1 and c_2):

$$\mu_1 = \frac{\partial g}{\partial c_1} - \kappa\nabla^2 c_1$$

$$\mu_2 = \frac{\partial g}{\partial c_1} - \kappa\nabla^2 c_2$$

The partial derivatives of the free energy expression g are:

$$g = ac_1^2c_3^2 + (c_1 + b)(c_2 - d)^2 + (e - c_1 - c_2)(c_2 - f)^2$$

$$\frac{\partial g}{\partial c_1} = 2ac_1c_3^2 - 2ac_1^2c_3 + (c_2 - d)^2 - (c_2 - f)^2$$

$$\frac{\partial g}{\partial c_2} = -2ac_1^2c_3 + (c_1 + b) * 2 * (c_2 - d) - (c_2 - f)^2 + 2(c_2 - f)(e - c_1 - c_2)$$

The concentrations are converted into dimensionless form:

$$\mu_1 = \frac{\partial g}{\partial c_1} - \frac{\kappa c_B}{L^2}\widehat{\nabla}^2(\hat{c}_1)$$

$$\mu_2 = \frac{\partial g}{\partial c_2} - \frac{\kappa c_B}{L^2}\widehat{\nabla}^2(\hat{c}_2)$$

$$\frac{\partial g}{\partial c_1} = 2a\hat{c}_1\hat{c}_3^2c_B^3 - 2a\hat{c}_1^2\hat{c}_3c_B^3 + (\hat{c}_2c_B - d)^2 - (\hat{c}_2c_B - f)^2$$

$$\frac{\partial g}{\partial c_2} = -2a\hat{c}_1^2\hat{c}_3c_B^3 + (\hat{c}_1c_B + b) * 2 * (\hat{c}_2c_B - d) - (\hat{c}_2c_B - f)^2 + 2(\hat{c}_2c_B - f)(e - \hat{c}_1c_B - \hat{c}_2c_B)$$

Scaling of chemical potential equation:

1. Multiply second term by ξ^2/ξ^2

$$\mu_1 = \frac{\partial g}{\partial c_1} - \frac{\kappa c_B}{L^2}\widehat{\nabla}^2(\hat{c}_1) * \frac{\xi^2}{\xi^2}$$

$$\mu_2 = \frac{\partial g}{\partial c_2} - \frac{\kappa c_B}{L^2}\widehat{\nabla}^2(\hat{c}_2) * \frac{\xi^2}{\xi^2}$$

2. Simplify with C_h number

$$\mu_1 = \frac{\partial g}{\partial c_1} - \frac{\kappa c_B c_h^2}{\xi^2}\widehat{\nabla}^2(\hat{c}_1)$$

$$\mu_2 = \frac{\partial g}{\partial c_2} - \frac{\kappa c_B c_h^2}{\xi^2}\widehat{\nabla}^2(\hat{c}_2)$$

3. Divide both sides by $\frac{\kappa c_B}{\xi^2}$, the scaling value for chemical potential and free energy

$$\mu_1 / \left[\frac{\kappa c_B}{\xi^2}\right] = \left[\frac{\partial g}{\partial c_1}\right] / \left[\frac{\kappa c_B}{\xi^2}\right] - c_h^2\widehat{\nabla}^2(\hat{c}_1)$$

$$\mu_2 / \left[\frac{\kappa c_B}{\xi^2}\right] = \left[\frac{\partial g}{\partial c_2}\right] / \left[\frac{\kappa c_B}{\xi^2}\right] - c_h^2\widehat{\nabla}^2(\hat{c}_2)$$

$$\widehat{\mu_1} = \frac{\widehat{\partial g}}{\partial c_1} - c_h^2\widehat{\nabla}^2(\hat{c}_1)$$

$$\widehat{\mu_2} = \frac{\widehat{\partial g}}{\partial c_2} - c_h^2\widehat{\nabla}^2(\hat{c}_2)$$

Without simplification, the chemical potential expressions defined by Alfarraj and Nauman are:

$$\mu_1 = (1 - c_1)\nabla\left(\frac{\delta G}{\delta c_1}\right) - c_2\nabla\left(\frac{\delta G}{\delta c_2}\right) - c_3\nabla\left(\frac{\partial g}{\partial c_3}\right)$$

$$\mu_2 = (1 - c_2)\nabla\left(\frac{\delta G}{\delta c_2}\right) - c_1\nabla\left(\frac{\delta G}{\delta c_1}\right) - c_3\nabla\left(\frac{\partial g}{\partial c_3}\right)$$

$$\mu_1 = (1 - c_1)\nabla\left(\frac{\partial g}{\partial c_1} - \kappa_1\nabla^2 c_1 - \kappa_3\nabla^2 c_2\right) - c_2\nabla\left(\frac{\partial g}{\partial c_2} - \kappa_3\nabla^2 c_1 - \kappa_2\nabla^2 c_2\right) - c_3\nabla\left(\frac{\partial g}{\partial c_3}\right)$$

$$\mu_2 = (1 - c_2)\nabla\left(\frac{\partial g}{\partial c_2} - \kappa_3\nabla^2 c_1 - \kappa_2\nabla^2 c_2\right) - c_1\nabla\left(\frac{\partial g}{\partial c_1} - \kappa_1\nabla^2 c_1 - \kappa_3\nabla^2 c_2\right) - c_3\nabla\left(\frac{\partial g}{\partial c_3}\right)$$

Since $\frac{\partial g}{\partial c_3}$ = 0, the last term can be neglected. Let $\kappa_1 = \kappa_2 = \kappa_3 = \kappa$.

The concentrations are converted into dimensionless form:

$$\mu_1 = (1 - \hat{c}_1 c_B)\nabla\left(\frac{\partial g}{\partial c_1} - \frac{\kappa c_B}{L^2}\widehat{\nabla}^2(\hat{c}_1) - \frac{\kappa c_B}{L^2}\widehat{\nabla}^2(\hat{c}_2)\right) - \hat{c}_2 c_B\nabla\left(\frac{\partial g}{\partial c_2} - \frac{\kappa c_B}{L^2}\widehat{\nabla}^2(\hat{c}_1) - \frac{\kappa c_B}{L^2}\widehat{\nabla}^2(\hat{c}_2)\right)$$

$$\mu_2 = (1 - \hat{c}_2 c_B)\nabla\left(\frac{\partial g}{\partial c_2} - \frac{\kappa c_B}{L^2}\widehat{\nabla}^2(\hat{c}_1) - \frac{\kappa c_B}{L^2}\widehat{\nabla}^2(\hat{c}_2)\right) - \hat{c}_1 c_B\nabla\left(\frac{\partial g}{\partial c_1} - \frac{\kappa c_B}{L^2}\widehat{\nabla}^2(\hat{c}_1) - \frac{\kappa c_B}{L^2}\widehat{\nabla}^2(\hat{c}_2)\right)$$

The expressions are simplified with the C_h number:

$$\mu_1 = (1-\hat{c}_1 c_B)\nabla\left(\frac{\partial g}{\partial c_1} - \frac{\kappa c_B}{L^2}\widehat{\nabla}^2(\hat{c}_1) * \frac{\xi^2}{\xi^2} - \frac{\kappa c_B}{L^2}\widehat{\nabla}^2(\hat{c}_2) * \frac{\xi^2}{\xi^2}\right)$$

$$- \hat{c}_2 c_B \nabla\left(\frac{\partial g}{\partial c_2} - \frac{\kappa c_B}{L^2}\widehat{\nabla}^2(\hat{c}_1) * \frac{\xi^2}{\xi^2} - \frac{\kappa c_B}{L^2}\widehat{\nabla}^2(\hat{c}_2) * \frac{\xi^2}{\xi^2}\right)$$

$$\mu_2 = (1-\hat{c}_2 c_B)\nabla\left(\frac{\partial g}{\partial c_2} - \frac{\kappa c_B}{L^2}\widehat{\nabla}^2(\hat{c}_1) * \frac{\xi^2}{\xi^2} - \frac{\kappa c_B}{L^2}\widehat{\nabla}^2(\hat{c}_2) * \frac{\xi^2}{\xi^2}\right)$$

$$- \hat{c}_1 c_B \nabla\left(\frac{\partial g}{\partial c_1} - \frac{\kappa c_B}{L^2}\widehat{\nabla}^2(\hat{c}_1) * \frac{\xi^2}{\xi^2} - \frac{\kappa c_B}{L^2}\widehat{\nabla}^2(\hat{c}_2) * \frac{\xi^2}{\xi^2}\right)$$

$$\mu_1 = (1-\hat{c}_1 c_B)\nabla\left(\frac{\partial g}{\partial c_1} - \frac{\kappa c_B c_h^2}{\xi^2}\widehat{\nabla}^2(\hat{c}_1) - \frac{\kappa c_B c_h^2}{\xi^2}\widehat{\nabla}^2(\hat{c}_2)\right)$$

$$- \hat{c}_2 c_B \nabla\left(\frac{\partial g}{\partial c_2} - \frac{\kappa c_B c_h^2}{\xi^2}\widehat{\nabla}^2(\hat{c}_1) - \frac{\kappa c_B c_h^2}{\xi^2}\widehat{\nabla}^2(\hat{c}_2)\right)$$

$$\mu_2 = (1-\hat{c}_2 c_B)\nabla\left(\frac{\partial g}{\partial c_2} - \frac{\kappa c_B c_h^2}{\xi^2}\widehat{\nabla}^2(\hat{c}_1) - \frac{\kappa c_B c_h^2}{\xi^2}\widehat{\nabla}^2(\hat{c}_2)\right)$$

$$- \hat{c}_1 c_B \nabla\left(\frac{\partial g}{\partial c_1} - \frac{\kappa c_B c_h^2}{\xi^2}\widehat{\nabla}^2(\hat{c}_1) - \frac{\kappa c_B c_h^2}{\xi^2}\widehat{\nabla}^2(\hat{c}_2)\right)$$

The scaling value of chemical potential is $\frac{\kappa c_B}{\xi^2}$:

$$\mu_1 / \frac{\kappa c_B}{\xi^2} = (1-\hat{c}_1 c_B)\nabla\left(\frac{\partial g}{\partial c_1} / \frac{\kappa c_B}{\xi^2} - c_h^2\widehat{\nabla}^2(\hat{c}_1) - c_h^2\widehat{\nabla}^2(\hat{c}_2)\right)$$

$$- \hat{c}_2 c_B \nabla\left(\frac{\partial g}{\partial c_2} / \frac{\kappa c_B}{\xi^2} - c_h^2\widehat{\nabla}^2(\hat{c}_1) - c_h^2\widehat{\nabla}^2(\hat{c}_2)\right)$$

$$\mu_2 / \frac{\kappa c_B}{\xi^2} = (1-\hat{c}_2 c_B)\nabla\left(\frac{\partial g}{\partial c_2} / \frac{\kappa c_B}{\xi^2} - c_h^2\widehat{\nabla}^2(\hat{c}_1) - c_h^2\widehat{\nabla}^2(\hat{c}_2)\right)$$

$$- \hat{c}_1 c_B \nabla\left(\frac{\partial g}{\partial c_1} / \frac{\kappa c_B}{\xi^2} - c_h^2\widehat{\nabla}^2(\hat{c}_1) - c_h^2\widehat{\nabla}^2(\hat{c}_2)\right)$$

$$\widehat{\mu_1} = (1-\hat{c}_1 c_B)\nabla\left(\frac{\widehat{\partial g}}{\partial c_1} - c_h^2\widehat{\nabla}^2(\hat{c}_1) - c_h^2\widehat{\nabla}^2(\hat{c}_2)\right) - \hat{c}_2 c_B \nabla\left(\frac{\widehat{\partial g}}{\partial c_2} - c_h^2\widehat{\nabla}^2(\hat{c}_1) - c_h^2\widehat{\nabla}^2(\hat{c}_2)\right)$$

$$\widehat{\mu_2} = (1 - \hat{c}_2 c_B)\nabla\left(\frac{\widehat{\partial g}}{\partial c_2} - c_h^2\widehat{\nabla}^2(\hat{c}_1) - c_h^2\widehat{\nabla}^2(\hat{c}_2)\right) - \hat{c}_1 c_B \nabla\left(\frac{\widehat{\partial g}}{\partial c_1} - c_h^2\widehat{\nabla}^2(\hat{c}_1) - c_h^2\widehat{\nabla}^2(\hat{c}_2)\right)$$

D. References

[1] *Breaking the Chemical and Engineering Barriers to Lignocellulosic Biofuels: Next Generation of Hydrocarbon Biorefineries.* A research roadmap for making lignocellulosic biofuels from the University of Massachusetts Amherst; June 25-26, 2007 Workshop, Washington DC.

[2] Public Law 110–140. (2007). Energy Independence and Security Act of 2007, http://leahy.senate.gov/issues/FuelPrices/EnergyIndependenceAct.pdf.

[3] Food vs. Fuel: FAQ. http://www.biodieselsustainability.com/faq.html

[4] Benefits of Biodiesel
http://www.biodiesel.org/pdf_files/fuelfactsheets/Benefits%20of%20Biodiesel.pdf

[5] Biodiesel Performance. http://www.biodiesel.org/pdf_files/fuelfactsheets/Performance.pdf

[6] Biodiesel Commonly Asked Questions.
http://www.biodiesel.org/pdf_files/fuelfactsheets/CommonlyAsked.pdf

[7] Lines, Michael. Biodiesel Reactor Modeling Using Matlab. Master's Thesis, University of Connecticut, 2008.

[8] Boucher, Matthew B., et al. Pilot Scale Two-phase Continuous Flow Biodiesel Production via Novel Laminar Flow Reactor-Separator. *Energy & Fuels*, **2009**, 23, 2750-2756.

[9] Chakulski, Brian. A Continuous Flow, Multi-Phase Reaction Model for Biodiesel Production. Master's Thesis, University of Connecticut, 2009.

[10] Badalassi, V.E. et al. Computation of multiphase systems with phase field models. *Journal of Computational Physics,* **2003,** 190, 371-397.

[11] Double-Well Potential. Dr. Frederick Phelan, NIST, available upon request.

[12] Kim, J., K. Kang, and J. Lowengrub, Conservative multigrid methods for ternary Cahn-Hilliard systems. *Commun. Math. Sci.*, **2004**, 2, 53-77.

[13] Tufano, C, et al. Effects of partial miscibility on drop-wall and drop-drop interactions. *J. Rheol.,* **2010***,* 54, 159-183.

[14] Kim, J., and J. Lowengrub. Phase field modeling and simulation of three-phase flows. *Interfaces Free Boundaries*, **2005**, 7, 435–466.

[15] Multicomponent Diffusion in Phase Separated Systems. Dr. Phelan, NIST, available upon request.

[16] Alfarraj, A. A., Nauman, B. E. Spinodal Decomposition in Ternary Systems with Significantly Different Component Diffusivities. *Macromolecular Theory and Simulations*, **2007**, 627-631.

[17] Alfarraj, A. A., Nauman, B. E. Gradient Energy Parameters for Polymer-Polymer-Solvent Systems and Their Application to Spinodal Decomposition in True Ternary Systems. *Journal of Polymer Science: Part B Polymer Physics*, **1990**, 28, 2395-2409.

[18] Bates, P.W., Fife, P.C. The dynamics of nucleation for the Cahn–Hilliard equation. *SIAM J. Appl. Math., **1993**,* 53 990.

[19] Hohenberg, P.C., Halperin, B.I. Theory of dynamic critical phenomena, Rev. Mod. Phys. **1977**, 47 (3), 435.

[20] Khatavkar, V.V. et al. On scaling of diffuse-interface models. *Chem. Eng. Sci., **2006**,* 61, 2364-2378.

[21] Bray, A.J. Theory of phase-ordering kinetics, *Adv. Phys*., **1994**, 43 (3), 357–459.

[22] Navier-Stokes Cahn-Hilliard Formulation. Dr. Phelan, NIST, available upon request.